MAGNET MODEL STUDIES FOR SEPARATED-SECTOR HEAVY ION CYCLOTRONS

E. D. Hudson, R. S. Lord, L. L. Riedinger, J. A. Martin, J. K. Bair, L. N. Howell, F. Irwin, J. W. Johnson, G. S. McNeilly, and S. W. Mosko

Oak Ridge National Laboratory,* Oak Ridge, Tennessee 37830, USA

M. A. Barre, M. P. Bourgarel, T. T. Luong and M. Ohayon

GANIL, France

Abstract

A four-sector model of a 2400 ton (2200 metric ton), K=440, separated-sector cyclotron magnet has been built to 0.15 scale. The sector angle of the magnet is 52°. Magnetic field measurements have been made using a single Hall-effect element that was positioned by a high-precision numerically controlled table. Magnetic field data and the ion focusing characteristics are presented.

1. Introduction

This paper describes the physical and magnetic field characteristics of a 0.15-scale model of the magnet for a K=440 MeV separated-sector cyclotron.[1,2] A list of the model and full-scale characteristics is given in Table 1. The K=440 cyclotron was proposed as the second stage accelerator to follow a 20 MV tandem electrostatic accelerator. With the shift to a 25 MV tandem, the size of the booster cyclotron has been reduced to K=300. Thus the model studies described in the paper do not precisely relate to the currently proposed booster.[3] Changes in the model will be made to more closely approximate a K=300 machine. These measurements were also made to provide magnetic field design information for the GANIL project.[4]

Table 1. Magnet Characteristics

	0.15 Scale Model (cm)	0.15 Scale Model (in.)	Full Scale Magnet (cm)	Full Scale Magnet (in.)
Energy constant (K), MeV			440	
Energy gain			9-19	
Magnetic field, kG	16		16	
Number of sectors	4		4	
Sector angle of magnet, deg.	52		52	
Gap	1.5	0.6	10.2	4
Pole radius				
minimum	6.1	2.4	40.6	16
maximum	53.7	21.15	358.0	141.0
Yoke radius, maximum	85.9	33.8	572.8	225.5
Yoke width	49.9	19.65	332.7	131.0
Yoke height	83.1	32.7	553.7	218.0
Sector weight				
tons	2.0		600	
metric tons	1.8		540	
Beam extraction radius			328.9	129.5
ρ at injection				
minimum			43.2	17.0
maximum			63	24.8
ρ at extraction			188.7	74.3
Ampere turns per sector, @ 16 kG	22,200		148,000	
Power per sector, kW	15		100	

*Operated by Union Carbide Corporation for the U.S. Energy Research and Development Administration.

2. Model Magnet

A plan view drawing of one of the four 52° sector magnets is in Fig. 1. The profile of the pole edge is also in this figure. The 0.5 inch radius of the pole edge and the two 0.6 inch steps in the pole edge were selected to give a coarse approximation to the Rogowski profile. The first step provides a space inside the vacuum enclosure for the leads of the trim coils, and the second step provides a surface for the vacuum seal. The coil cores and the yoke subtend a full 52°. A photograph of the model, the probe positioner, and the field measuring equipment is shown in Fig. 2. The aluminum support structure for the four-sector magnets was mounted on the base for the probe positioner table, and provided magnetic isolation between the magnets and the steel base. The magnets were leveled and aligned using precision optical procedures. Aluminum brackets were provided on each yoke for mounting the optical instruments. A sharp needle for use as an optical target was mounted at the center on a brass plate supported by the four

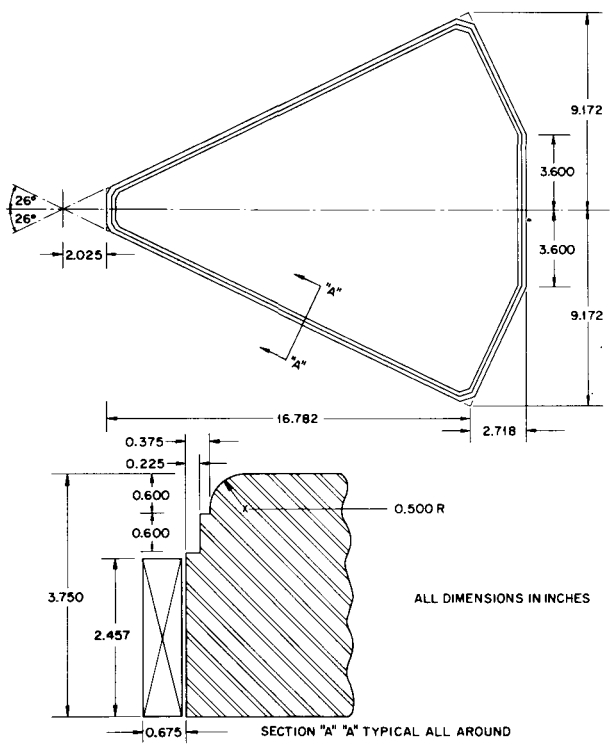

Fig. 1. Profile and plan view of one of the four 52° sector magnet poles for the 0.15-scale model.

Proc. 7th Int. Conf. on Cyclotrons and their Applications (Birkhäuser, Basel, 1975), p. 197-200

magnet yokes. The same brass plate with a larger steel spike to give a cone-shaped magnetic field was used later to position the Hall probe at the center of the system.

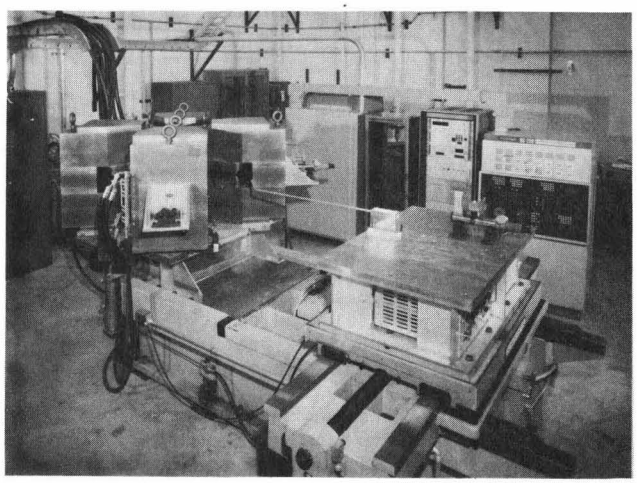

Fig. 2. Photograph of the model magnet system, the table and milling machine, and the electronics used in the data acquisition.

The coils for the model were wound from 0.187 inch square copper conductor with a 0.125-in.-square water passage. Each coil was composed of 36 turns separated into two units so that a series-parallel connection could be used to match the available power supplies. The steel cap pieces above and below the coil slots on the yoke are provided to aid in assembly of the laminations of the full-scale magnet. The lower cap provides a precision surface for assembly; the upper cap is included to preserve magnetic symmetry.

3. Instrumentation

A single F. W. Bell Hall probe (BHT-910) was mounted on an aluminum arm with vibration dampers and positioned by a high-precision numerically controlled table to within ± 0.001 in. The table is a precision machine tool that was adapted for field measurements. The table was programmed to move radially in 143 steps of 0.150 inches (1 inch full scale) from the center of the magnet system to the maximum radius of 21.45 inches. The Hall voltage was measured and recorded on magnetic tape at the center and at each increment in radius. After each radial scan the probe returned to the center (r=0) to allow verification of the position with an alignment telescope. In general the positioning accuracy of the table was quite good and thus the Hall probe returned to within 0.001 inch of the center. Successive radial scans were taken in one degree azimuthal steps from $\theta=0°$, the center of the sector magnet (hill), to 45°, the center of the space between the sectors (valley). In addition to field measurements at 6624 positions, we also recorded the Hall drive current and magnet shunt currents on magnetic tape at the beginning of each radial scan. At the end of a complete radial map of the field in this 45° section, azimuthal scans were taken to check pole symmetry and alignment. Hall voltages were recorded as the probe was moved in 1° steps from 45° (center of the valley) to -30° at radii of 6 and 7.8 inches, and then in similar steps from +45° to -45° (center of another valley) at model radii of 9.6, 11.4, 13.2, and 15 inches. Approximately 3.5 seconds were required for the positioning of the table and recording of the Hall voltage at each of these 7140 positions. A period of 8-9 hours was required for the complete radial map followed by the azimuthal symmetry checks.

The magnetic center of the Hall probe was located by making a series of scans over a steel spike mounted at the center of the magnet system. The Hall voltages were recorded as the probe was moved in 0.004 inch steps from -0.200 inches to +0.200 inches relative to the approximate center; this was done first in one direction and then in an orthogonal direction. A 2.4-inch long spike (used for centering only) had a base diameter of 0.77 inch and produced a field bump of 233 gauss. We conclude that the center of the Hall probe had been found to an accuracy within 0.001 inch. After the center had been found magnetically, a telescope was mounted to provide a visual check of the probe position after each radial scan.

A block diagram of the data acquisition system is shown in Fig. 3. The Hall probe is positioned by a rectilinear, logic controlled positioner, which is a modified paper-tape controlled milling machine.

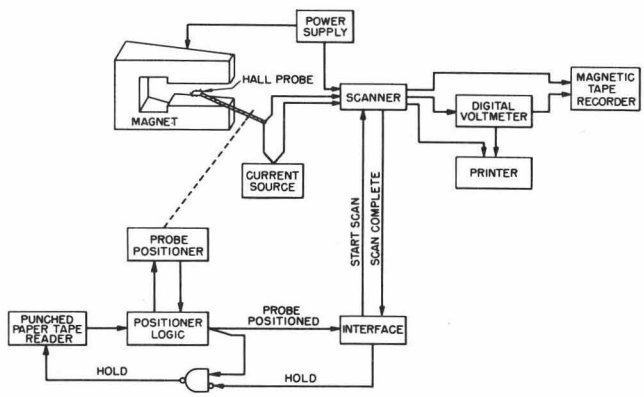

Fig. 3. Block diagram of the data acquisition system.

A computer program was written to convert from the desired movements on a polar grid to the corresponding X and Y increments. This program also prepares a punched paper tape containing a series of commands in the proper format to move the table in radial or azimuthal directions. Data from the punched paper tape is fed to the positioner logic unit which generates an incremental motion command. Feedback from the positioner to the logic unit indicates when the Hall probe is positioned. An "in position" signal from the logic unit triggers the "interface unit;" then a "start" signal is transmitted to the data scanner and a "hold" signal is generated for the tape reader. On completion of the scan cycle, the scanner transmits a reset signal to the interface. When the hold signal from the interface resets and

the positioner logic unit is indicating "probe positioned," the "hold" gate on the paper tape reader resets, and the next position information is read. The analog output from the scanner is read by a digital voltmeter (DVM). The digital output from the DVM and the scanner's channel number are recorded both on magnetic tape and on printed paper tape. The magnetic tape is read directly by a computer while the printed data are used for manual data verification.

The Hall probe was calibrated by comparison with the output of an NMR probe positioned adjacent to the Hall probe in a uniform field. The seventh-order polynomial relating the Hall voltage and the magnetic field was fit to the data and was found to be quite accurate over a range of 1 to 21 kG.

The magnetic tape containing the field data was read and analyzed on the SEL-840-A computer, the main computer of the ORIC laboratory. These voltages were converted to magnetic field values at this point and a large 144 x 90 array of field values was created on disk for storage and analysis. The data taken in radial scans were sorted so that the array contained 144 radial groups of azimuthal data. The 44 data points taken from 1° to 44° were folded over to create a 90 point azimuthal profile from the center of one hill (0°) to 1° before the center of another hill (89°). The average magnetic field as a function of radius and the magnetic angle of the sector were calculated directly from the array.

This large array of field values was stored on magnetic tape for future reference and also transmitted by a telephone link to a disk at the IBM 360/91, the central ORNL computer. The General Orbit Code then used the field data to calculate equilibrium orbits for various particles.

4. Results

The magnetic field profile of our model was experimentally mapped at excitation levels of 5, 8, 12, 14, 16, and 18 kG. The data are quite good, in that the field profiles constructed from different radial scans are very smooth. Fig. 4 displays a normalized comparison of the average magnetic field as a function of radius for 8 and 16 kG. This average at each point has been calculated along a path of constant radius rather than along the particle path. It is gratifying that the average is smooth to within 0.01% of the maximum field, that is 1 or 2 gauss out of 16 kG. Between the limits of the injection and extraction radii, the 8 and 16 kG fields are similar in shape to within 0.5%. The near absence of saturation effects at 16 kG, the operating point of the full-scale magnet, leads to very nearly the same dynamics of particle orbits at low and high field levels.

The azimuthal profile of the 16 kG field at 4 different radii is shown in Fig. 5. The inset in the figure contains the calculated magnetic angle at each radius. The very good agreement between these calculated values and the design value of 52° demonstrates that the steps around the pole edge provide an excellent approximation of the desired Rogowski profile. The constancy of the magnetic angle as a function of radius also demonstrates the success of the design. We find, in addition, that the magnetic angle at a given radius is constant to within 0.5° from 8 to 18 kG. This once again shows the near absence of saturation effects over this important range.

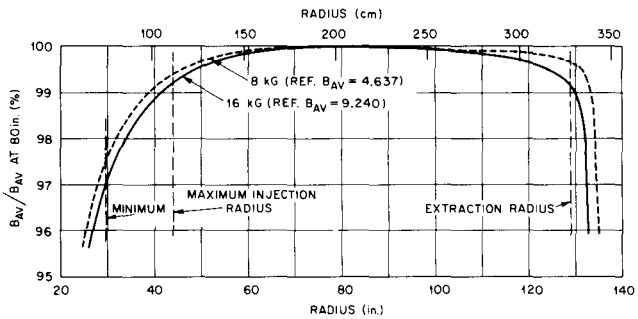

Fig. 4. Average magnetic field as a function of full-scale radius for the 8 and 16 kG fields. Note that there is at most 0.5% difference in field shape between the two in the range between the injection and extraction radii.

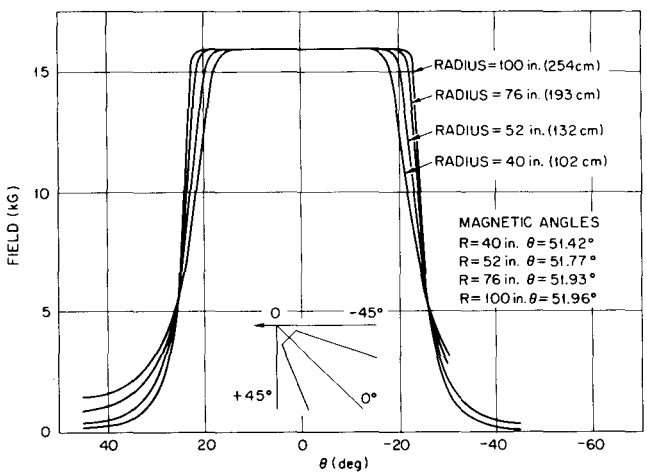

Fig. 5. Magnetic field versus angle at different radii for the 16-kG map. The magnetic angles calculated from these data are also shown.

Radial scans of the 16 kG field at various angles are presented in Fig. 6. This diagram excludes intermediate radii in order to emphasize the gradient encountered at large and small radii. Of special significance is the 45° curve, which describes the field along the center of the valley. At small radii, this field approaches 3 kG, which must be traversed by the injected beam.

The results of General Orbit Code calculations with $^{12}C^{6+}$ and $^{238}U^{36+}$ injected into the 16 kG field are graphed in Fig. 7. Here the orbits at successive radii were isochronized by adjusting the field level as a function of radius, with this difference eventually furnished by trimming coils. This

resonance diagram demonstrates the operating region of the proposed cyclotron and shows that with the 52° sector we will be free of instabilities caused by the essential resonances. Table 2 displays a partial listing of the final output of the General Orbit Code after 10 isochronization iterations. Only every fifth step in energy has been listed for ^{12}C and ^{238}U. The range of ν_r and ν_z values is, once again, quite satisfactory for the successful operation of a four-sector cyclotron.

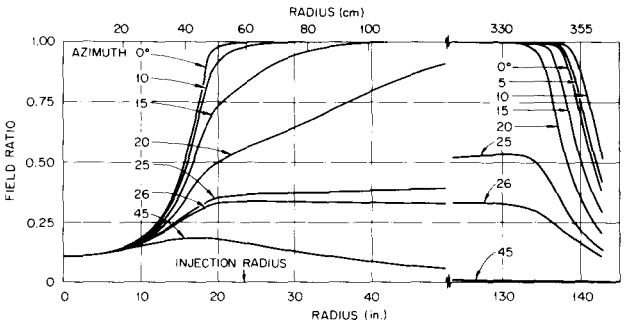

Fig. 6. Field ratio from the 16-kG map as a function of full-scale radius at different azimuths.

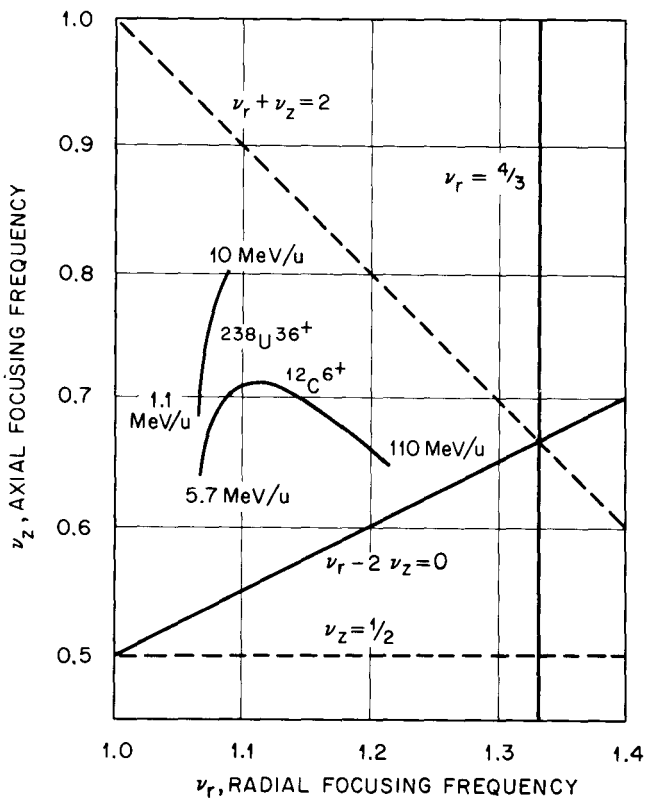

Fig. 7. Resonance diagram describing acceleration of ^{12}C and ^{238}U.

Table 2. Results of Orbit Calculations of the Focusing Frequencies for ^{238}U and ^{12}C

E (MeV)	Req	PReq	T	Rave (in.)	Ramp (in.)	νr	νz
$^{238}U^{36+}$:							
266	0.0511	0.00	0.99999	41.8	2.4	1.0683	0.6909
441	0.0657	0.00	0.99999	53.8	3.3	1.0695	0.7263
616	0.0776	0.00	0.99995	63.5	3.9	1.0724	0.7447
791	0.0879	0.00	1.00004	71.9	4.5	1.0746	0.7566
966	0.0971	0.00	0.99999	79.4	5.0	1.0747	0.7659
1141	0.1055	0.00	1.00001	86.2	5.5	1.0774	0.7708
1316	0.1132	0.00	0.99995	92.5	5.9	1.0767	0.7785
1491	0.1205	0.00	0.99998	98.4	6.3	1.0486	0.7755
1666	0.1273	0.00	0.99995	104.0	6.7	1.0844	0.7808
1841	0.1337	0.00	0.99995	109.2	7.0	1.0818	0.7875
2016	0.1398	0.00	0.99998	114.2	7.3	1.0843	0.7903
2191	0.1457	0.00	0.99996	119.0	7.7	1.0835	0.7954
2366	0.1513	0.00	0.99999	123.6	8.0	1.0897	0.7942
$^{12}C^{6+}$:							
68	0.1146	0.00	0.99990	30.4	1.7	1.0678	0.6422
168	0.1790	0.00	0.99988	47.4	2.8	1.0820	0.6849
268	0.2246	0.00	0.99985	59.4	3.6	1.0966	0.7087
368	0.2615	0.00	0.99987	69.1	4.3	1.1107	0.7099
468	0.2930	0.00	0.99979	77.4	4.9	1.1226	0.7101
568	0.3208	0.00	0.99986	84.8	5.4	1.1307	0.7097
668	0.3457	0.00	0.99987	91.3	5.8	1.1498	0.6934
768	0.3684	0.00	0.99988	97.3	6.2	1.1549	0.6965
868	0.3892	0.00	0.99987	102.8	6.6	1.1674	0.6858
968	0.4085	0.00	0.99987	107.9	6.9	1.1808	0.6744
1068	0.4266	0.00	0.99989	112.6	7.3	1.1912	0.6649
1168	0.4434	0.00	0.99993	117.1	7.6	1.2007	0.6587
1268	0.4593	0.00	0.99998	121.3	7.9	1.2142	0.6481
1328	0.4684	0.00	0.99995	123.6	8.0	1.2189	0.6445

Acknowledgements

The authors wish to thank K. N. Fischer, M. L. Brewer, C. A. Ludemann, and D. C. Hensley for their assistance on the computer processing of the data.

References

1. J. A. Martin, et al., AIP Conference Proceedings, No. 9, Cyclotrons - 1972, 54, American Institute of Physics (1972).

2. E. D. Hudson, et al., IEEE Trans. Nucl. Sci. NS-20, No. 3 (1973)168.

3. S. W. Mosko, et al., "A Separated-Sector Cyclotron Post-Accelerator for the Oak Ridge Heavy Ion Laboratory," Proceedings of this conference.

4. The GANIL Study Group, IEEE Trans. Nucl. Sci. NS-22, No. 3 (1975) 1651.